Research Article | Vol. 28, No. 25 / 7 December 2020 / Optics Express 38115
Optics EXPRESS

Ethane detection with mid-infrared hollow-core fiber photothermal spectroscopy

FEIFAN CHEN,[1,2] SHOULIN JIANG,[2] WEI JIN,[1,2,*] HAIHONG BAO,[1,2] HOI LUT HO,[1,2] CHAO WANG,[1,3] AND SHOUFEI GAO[1]

[1]*Department of Electrical Engineering, The Hong Kong Polytechnic University, Hung Hom, Kowloon, Hong Kong, China*
[2]*Photonics Research Center, The Hong Kong Polytechnic University Shenzhen Research Institute, Shenzhen 518057, China*
[3]*School of Electrical Engineering and Automation, Wuhan University, Wuhan 430072, China*
[*]*eewjin@polyu.edu.hk*

Abstract: We report a compact mid-infrared (MIR) photothermal spectroscopic ethane (C_2H_6) sensor with a hollow-core negative-curvature-fiber (HC-NCF) gas cell. The HC-NCF supports low-loss transmission of an MIR pump (3.348 μm) and a near-infrared (NIR) probe (1.55 μm). The pump and probe laser beams are launched into the gas cell from the opposite ends of the HC-NCF, allowing independent MIR pump delivery and NIR fiber-optic probe circuitry. The use of Fabry-Perot as the probe interferometer simplifies the sensor design and suppresses the common-mode noise in the lead in/out single-mode fiber. With a 14-cm-long HC-NCF, an ethane sensor system with the limit of detection (LOD) of 13 parts-per-billion (ppb) is achieved with 1 s lock-in time constant. The LOD goes down to 2.6 ppb with 410 s average time, which corresponds to noise equivalent absorption (NEA) of 2.0×10^{-6} and is a record for the hollow-core fiber MIR gas sensors. The system instability is 2.2% over a period of 8 hours.

1. Introduction

As the most abundant non-methane hydrocarbon in the atmosphere and the second most abundant constituent of natural gas after methane, monitoring the ethane concentration is important for the research on atmospheric chemistry and the climate [1,2], as well as oil and gas prospecting [3]. The level of exhaled ethane provides a non-invasive, quantitative, and direct measure of lipid peroxidation, which is promising for identifying schizophrenia or lung cancers [4–6]. For these applications, the required limit of detection is on the level of parts-per-billion (ppb) or lower.

Patterson *et al.* reported an ethane sensor using tunable diode laser absorption spectroscopy (TDLAS) with a 3.3 μm cryogenically cooled lead-salt laser and a Herriot cell of ~ 200 m effective optical path length and achieved the limit of detection (LOD) as low as 70 parts-per-trillion (ppt) [7]. Sampaolo *et al.* demonstrated a compact ethane sensor with quartz-enhanced photoacoustic spectroscopy (QEPAS) and achieved LOD of 7 ppb at 200 Torr [8]. The QEPAS system uses an open-path photoacoustic gas cell and a resonant quartz-tuning-fork for acoustic detection, the mechanical movements of different components would degrade the system performance [9].

Photothermal interferometry (PTI) is a highly sensitive and selective technique for trace gas detection [10]. It uses a probe-pump configuration: absorption of pump beam results in localized heating, modulating the refractive index (RI) of the gas sample and hence the phase of a probe beam propagating through the gas sample. The phase modulation is detected by optical interferometry. The magnitude of the phase modulation is affected by a number of factors such as overlap of pump and probe fields, pump modulation frequency, temperature, pressure and humidity, and is proportional to gas concentration, absorption distance, and the intensity of the pump, assuming other parameters are kept constant [10,11]. Early PTI systems used free-space optics, and there is a compromise among the practically achievable absorption distance, the instrument size, and the complexity in optical alignments [10].

#410927 https://doi.org/10.1364/OE.410927
Journal © 2020 Received 24 Sep 2020; revised 19 Nov 2020; accepted 20 Nov 2020; published 2 Dec 2020

Optics EXPRESS

A hollow-core fiber (HCF) confines light and the gas sample simultaneously in the hollow-core, providing an ideal platform for strong light-gas interaction over a long distance [12,13]. We recently demonstrated gas detection using PTI with HCF gas cells operating in the NIR [13–17]. Compared with direct absorption spectroscopy (DAS) and wavelength modulation spectroscopy (WMS) using HCFs, PTI with HCFs is less affected by noise resulting from coherent mixing of the fiber modes and hence enables higher detection sensitivity [14]. Taking the advantages of the mature telecom fiber-optic components in the NIR, different fiber-optic phase-detection configurations such as Mach Zehnder interferometer (MZI) [14], Sagnac interferometer [15], Fabry-Perot interferometer (FPI) [16] and dual-mode interferometer [17], have been investigated for the detection of photothermal (PT) phase modulation. LOD down to ppb and sub-ppb levels have been demonstrated for gases (e.g., acetylene) with relatively strong absorption in the NIR.

However, gases like ethane do not have strong absorption at the NIR. To sensitively detect ethane with PTI, an MIR pump, at which ethane absorption is the strongest, may be used to generate PT phase modulation. At the same time, a highly sensitive fiber-optic probe interferometer at NIR is used to detect the phase modulation. This MIR-pump and NIR-probe scheme could be used to detect a range of gas molecules that have strong absorption in the 2 to 13 μm region. Li *et al.* [18] demonstrated the detection of N_2O with PTI using an inner-surface-coated hollow-capillary fiber, a 4.46-μm pump laser and an MZI operating at 1.55 μm, and achieved noise equivalent absorption (NEA) of 5.1×10^{-4}. Recently, Yao *et al.* [19] reported the detection of formaldehyde at 3.6 μm with a similar MZI but with a microstructured hollow-core negative-curvature-fiber (HC-NCF). The HC-NCF has a better transmission at both the pump and the probe wavelengths, which enabled a NEA of 9.2×10^{-5} with a 120-cm-long HC-NCF. However, for both systems, to couple the pump and probe simultaneously into the HCF, free-space optical components are used to form a hybrid fiber-optic/free-space MZI, which leads to instability and makes it difficult to use for practical field applications [20].

In this paper, we report a PTI ethane sensor with an HC-NCF gas cell, simple MIR optics to deliver pump power into the hollow-core, and a NIR all-fiber FPI to probe the PT phase modulation with high sensitivity. Among all the reported MIR HCF gas sensors, this sensor demonstrated impressive stability and the lowest NEA.

2. Design of gas cell

Figure 1(a) shows the calculated absorption lines of ethane and water in the spectral range from 2970 to 3000 cm^{-1}. We choose to work at the strongest line at 2986.72 cm^{-1}, and the calculated absorption coefficient and spectral linewidth at 296 K and 1 atm are respectively 5.5×10^{-4} cm^{-1} and 0.144 cm^{-1} for 10 ppm ethane. Figure 1(b) shows the measured absorption spectrum of 1% ethane balanced with N_2, by using direct absorption and a 14-cm-long HCF gas cell (black squares) in the lab environment. Lorentzian curve fitting shows the absorption linewidth is about 0.151 cm^{-1}, in good agreement with the calculated results based on the HITRAN database.

Figure 2 shows the construction of the HCF gas cell. It is made by mechanically splicing, using ceramic ferrules and sleeves, a 14-cm-long sensing HC-NCF (orange color) to two solid optical fibers (blue and red). Small gaps of several tens of micrometers are kept between the HC-NCF and the solid fibers, and the gas filling into the hollow-core is made via these gaps and the slot on the sleeves. The HC-NCF has a hollow-core of 65 μm in diameter, inscribing by a single ring of six non-touching silica capillaries [21,22], and the SEM cross-sectional image is shown in Fig. 2(b). This HCF has multiple transmission bands and the optical attenuations at 3.34 μm (the pump) and 1.55 μm (the probe) are ~ 0.4 dB/m and ~ 0.15 dB/m, respectively [22].

The red fiber is an MIR InF_3-based single-mode fiber (SMF) at the pump wavelength. It couples the pump beam into the HCF from one end to produce PT phase modulation, which may be expressed as:

$$\Delta\phi = k\alpha(\lambda_{pump})CLP_{pump} \quad (1)$$

Optics EXPRESS

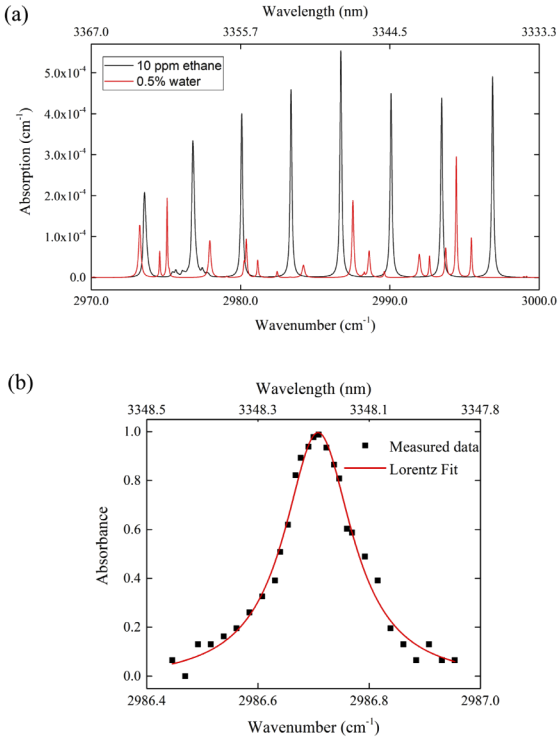

Fig. 1. (a) HITRAN-based absorption spectrum of 10 ppm ethane and 0.5% water from 2970 cm^{-1} to 3000 cm^{-1}. (b) Measured absorption spectrum around 2986.7 cm^{-1}.

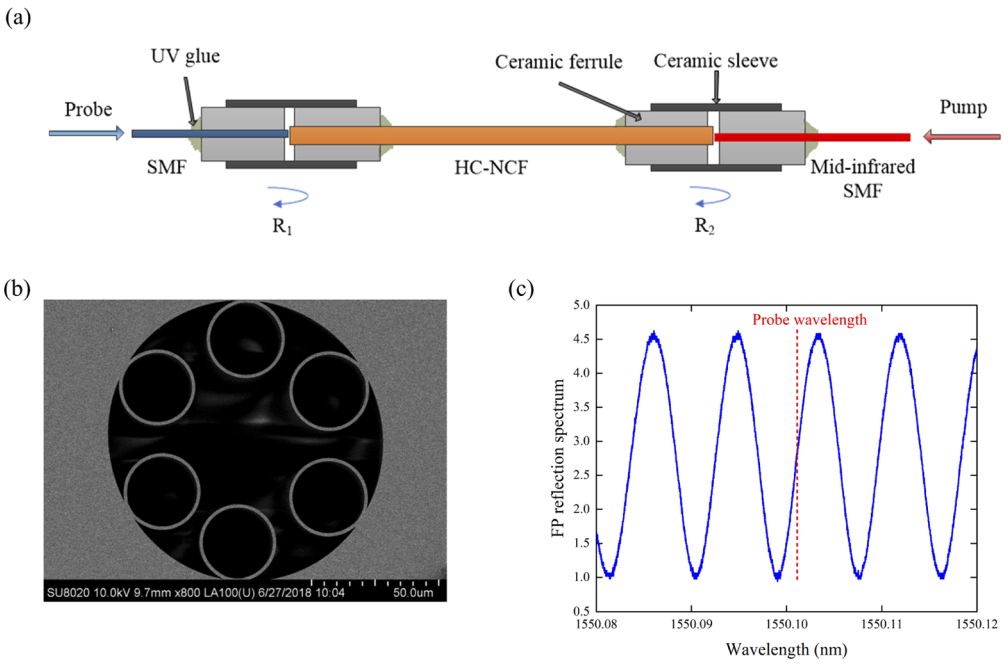

Fig. 2. (a) Schematic of the HC-NCF gas cell showing the pump input from the MIR fiber and the probe input to and reflections from the FPI. (b) Cross-section of the HC-NCF. (c) The measured reflection spectrum of the FPI.

Optics EXPRESS

where C is the gas concentration, $\alpha(\lambda_{pump})$ the absorption coefficient, λ_{pump} the pump wavelength, L the length of the HCF, P_{pump} the pump power in the hollow-core. k is a parameter related to fiber and gas parameters and depends on the frequency of the pump modulation. The mode field diameter (MFD) of the MIR SMF and HC-NCF at the pump wavelength are respectively 10.2 μm and 52 μm, and the joint loss for light transmission from the MIR fiber to the HC-NCF is about 3 dB.

The blue fiber is the standard SMF-28e fiber and it delivers the probe beam into the HCF from the other end of the HC-NCF gas cell and receives the reflected probe beams from the gas cell. As shown in Fig. 3, the pump and probe beams are launched into the HC-NCF from opposite ends, which enables complete separation of the pump and probe optics, allowing the use of extremely simple MIR optics to deliver pump power into the HCF for PT phase generation and cost-effective NIR components to form all-fiber circuity for highly sensitive detection of the PT phase modulation. The two natural reflections (~4%) at the SMF28/HC-NCF and HC-NCF/MIR-SMF joints form a low-finesse FPI for the probe beam. The reflected spectrum around 1550 nm was measured with a tunable narrow-linewidth laser in combination with an oscilloscope and is shown in Fig. 2(c). The free spectral range (FSR) is 8.6 pm, agreeing very well with the calculated value by using $\delta\lambda \approx \lambda^2/2L$. The MFDs of the SMF-28e and HC-NCF at the probe wavelength are respectively 10.4 μm and 49 μm. The measured joint loss is about 3 dB for light transmission from the SMF to the HC-NCF and 6 dB from the HC-NCF to SMF. The total coupling loss (α) for the probe beam reflected from the HC-NCF/MIR-SMF joint is about 9 dB. Considering the similar RIs of the SMF-28e (1.47) and the MIR-SMF (1.50), we may regard the reflectivity at the two interfaces as approximately the same, i.e., $R_1 \approx R_2 = R(R<<1)$. Neglecting the transmission loss of the HC-NCF, the reflected light intensity from the FPI may be approximated by [16]

$$I_R \approx I_o R[1 + \alpha^2 + 2\alpha \cdot \cos\varphi] \tag{2}$$

With

$$\varphi = \frac{4\pi n_{eff} d}{\lambda} + \varphi_0 \tag{3}$$

where I_0 and I_R are respectively the incident and reflected light intensities, φ is the phase difference between the two reflected beams, n_{eff} is the effective RI for the probe, d is the cavity length of FPI, λ is the probe wavelength, and φ_0 is a constant.

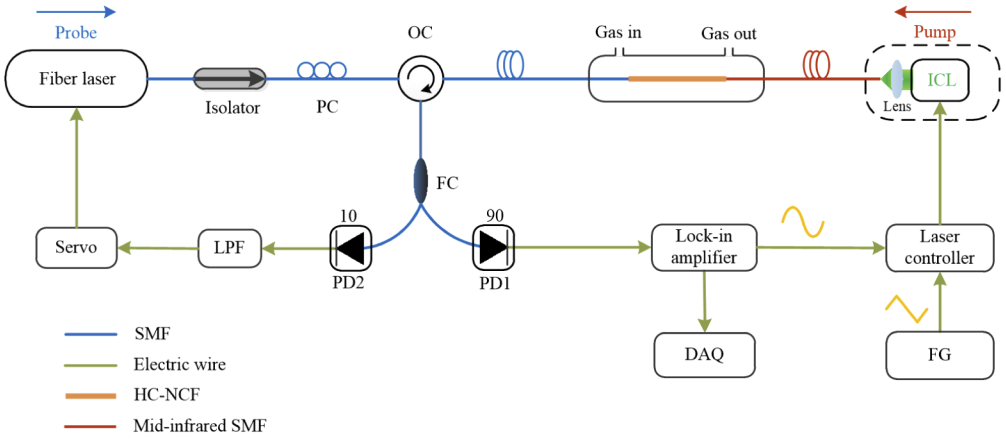

Fig. 3. Experiment set-up for ethane detection with 14-cm-long HC-NCF. DAQ, data acquisition; FC, fiber coupler; FG, function generator; ICL, interband cascade laser; LPF, low-pass-filter; OC, optical circulator; PC, polarization controller; PD, photodetector.

Optics EXPRESS

The fringe contrast [11] in the unit of dB may be expressed as

$$10\log_{10}\frac{I_{R,\max}+I_{R,\min}}{I_{R,\max}-I_{R,\min}} = 10\log_{10}\frac{1+\alpha^2+2\alpha}{1+\alpha^2-2\alpha} \tag{4}$$

For $\alpha = 9$ dB, the fringe contrast is calculated to be 6.4 dB, corresponding well with the measured value of ~ 6.5 dB, as shown in Fig. 2(c). There is room for further improvement by reducing the joint loss α.

For gas detection experiments, a narrow linewidth laser (see Section 3) is used as the probe source and the probe laser wavelength is locked to the quadrature point of the interference fringe so that the PT phase modulation is efficiently and linearly converted into intensity modulation at the FPI output.

3. Experimental set-up

The experimental set-up is shown in Fig. 3. A 3.4 μm interband cascade laser (ICL) with emission power up to 6 mW is used as the pump source and the collimated beam is coupled into the MIR SMF through an FC/APC connector by using a lens. The coupling efficiency into the MIR fiber is ~ 50%, corresponding to a pump power level of ~ 1.5 mW coupled into the HC-NCF. A 2f-WMS detection technique is employed in the experiment to improve the signal-to-noise ratio (SNR). The ICL is sinusoidally modulated at 7 kHz via a current controller. The wavelength modulation results in periodic absorption and heating of the gas sample, which modulates the phase of the probe beam. At the same time, the wavelength of the ICL is scanned via a temperature controller at 3 mHz, because the wavelength span of the ICL by current scanning is limited.

We use a single frequency fiber laser as the probe source and a polarization controller to maximize the fringe contrast of FPI. The fiber laser is equipped with a piezoelectric wavelength tuning mechanism and the probe wavelength can be servo-controlled so that the FPI is always operating at quadrature. From Fig. 2(c), the quadrature point corresponds to a voltage of V_{offset}=2.7 V, and we use the difference between the DC output of PD2 and this reference voltage, i.e. $V_{error} = V_{DC} - V_{offset}$, as the error signal. The error signal is sent into the servo controller, which generates the control signal to change the probe wavelength. The stabilization mechanism by using DC output and servo-loop ensures high sensitivity and long-term stability of the system. Servo-control of the probe wavelength instead of the cavity length [23] of the FPI enables completely passive all-fiber gas cells without electric connections. The FPI output is demodulated by a lock-in amplifier at the second harmonic of the modulation frequency.

4. Test and results

4.1. Performance of the servo-loop

Figure 4(a) shows the DC output detected by PD2 with and without servo-control. The output fluctuates considerably around the quadrature point without servo-control and reaches an approximately constant level immediately after the servo stabilization is applied. The performance of the FPI stabilization in terms of phase fluctuation from the quadrature point is calculated by comparing the output fluctuation with the interference fringe contrast in Fig. 2(c) and is shown in Fig. 4(b). The standard deviation (s.d.) of phase fluctuation is 0.054°, about an order of magnitude better than that of a stabilized MZI [14].

4.2. Optimal modulation frequency and depth

Figure 5(a) shows the measured second harmonic (2f) output signal of the FPI for varying modulation voltage when the HCF gas cell is filled with 1000 ppm ethane balanced with nitrogen. The experiments were conducted at room conditions. The pump laser is centered at 3348.15 nm and the modulation frequency is 7 kHz. The optimal modulation voltage is 45 mV, which

Optics EXPRESS

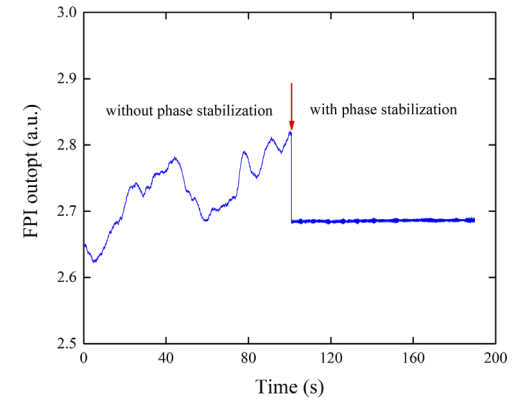

(a)

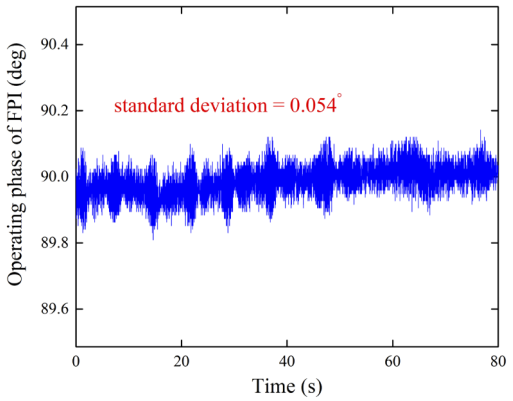

(b)

Fig. 4. FPI phase stabilization. (a) DC output of the FPI with and without phase stabilization. (b) Performance of FPI stabilization in terms of phase fluctuation around the quadrature point. The sampling frequency is 40 samples per second.

coincides well with an optimal modulation depth of 2.2 times the absorption linewidth considering the conversion coefficient of the current controller and the ICL.

Figure 5(b) shows the dependence of 2f output signal and noise level on the modulation frequency with the modulation voltage fixed at 45 mV. The 2f signal decreases with the increasing modulation frequency and the −3dB roll-off frequency is about 20 kHz, which is determined mainly by the thermal conduction process in the HCF and the ns-level relaxation time of ethane can be ignored [24]. The noise was also measured by filling the HCF with pure nitrogen at room condition. The best SNR is achieved around 7 kHz, as shown in the inset of the figure.

4.3. *Ethane detection with high sensitivity and stability*

Ethane detection experiments were conducted by filling different concentrations of ethane balanced with N_2 into the gas cell. The HCF gas cell was placed inside a gas chamber with a volume of about 1.8 L and the gas chamber was filled with gas sample through a flowmeter, whose outlet pressure is slightly higher than 1 atm. It took about 300 s for the signal to reach 90% of the maximum value with a flow rate of 500 standard cubic centimeter per minute (SCCM). The slow response is not limited by the HCF gas cell but by the size of the chamber, and can be

Optics EXPRESS

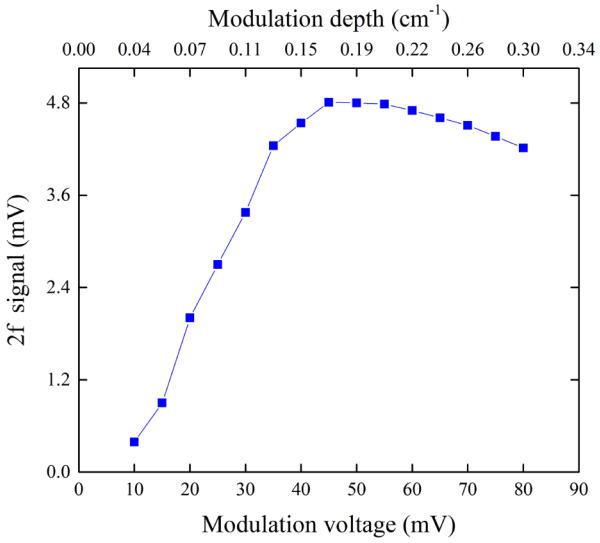

(a)

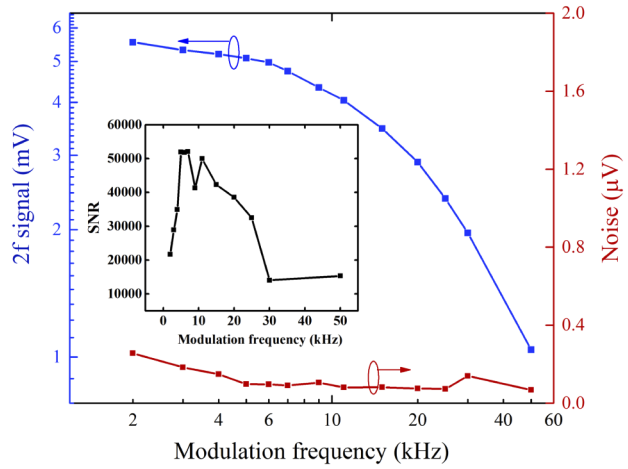

(b)

Fig. 5. (a) 2f output signal at the absorption line center as a function of modulation voltage. (b) 2f signal and the s.d. of the noise as functions of modulation frequency. The inset shows the SNR as a function of modulation frequency.

Optics EXPRESS

significantly shortened with a smaller chamber and/or by introducing microchannels along the HCF [25]. Figure 6(a) shows the 2f lock-in output with 1 ppm ethane filled into the HC-NCF and when the pump is tuned across the absorption line at 3348.15 nm. Figure 6(b) shows the s.d. of the noise over a period of 2 minutes, which was determined from the 2f lock-in output when the gas cell was filled with pure N_2. The s.d. of noise is 0.095 μV, giving an SNR of ~ 80 and a LOD of 13 ppb, corresponds to NEA of 1.0×10^{-5}, for an SNR of unity and 1 s lock-in time constant with filter slope of 18 dB/Oct, corresponding to a detection bandwidth of 0.094 Hz. This LOD is just 2 times higher than the shot-noise-limited NEA, which is calculated to be 5.0×10^{-6} [14].

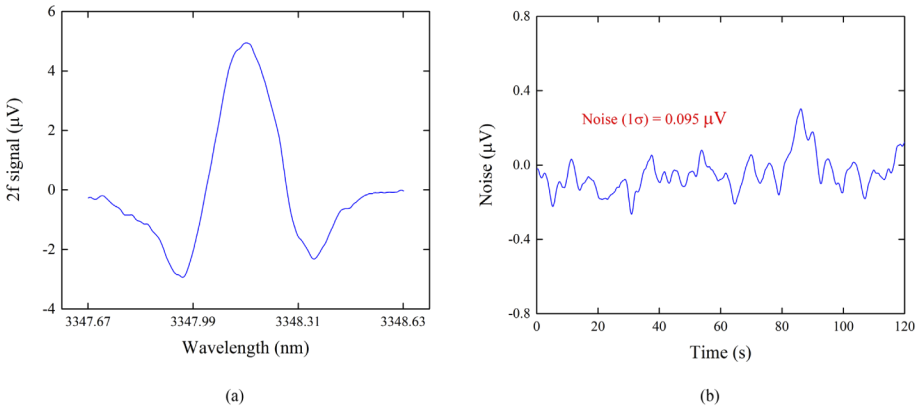

Fig. 6. (a) 2f lock-in output signal as a function of pump wavelength for 1 ppm ethane in nitrogen. (b) 2f signal when the gas cell was filled with pure nitrogen and the pump laser was fixed at 3348.15 nm.

Allan deviation analysis was conducted with the noise data over a period of 4 hours, and the results are shown in Fig. 7. The optimal averaging time τ is determined to be 410 s, at which the s.d. of noise is 0.019 μV, corresponding to a noise equivalent concentration (NEC) of 2.6 ppb ethane and a calculated NEA of 2.0×10^{-6}.

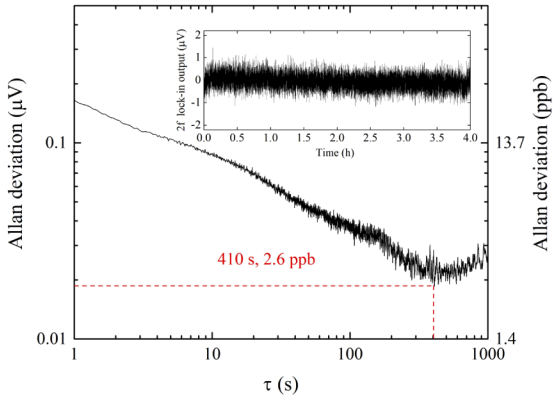

Fig. 7. Allan deviation analysis of the baseline noise over a period of 4 hours. The inset is the time trace. The time constant of the lock-in amplifier is 100 ms.

The peak-to-peak values of the 2f signal at different ethane concentrations are shown in Fig. 8. The 2f signal amplitude increases approximately linearly with the gas concentration with an R-square value of 0.9993.

Optics EXPRESS

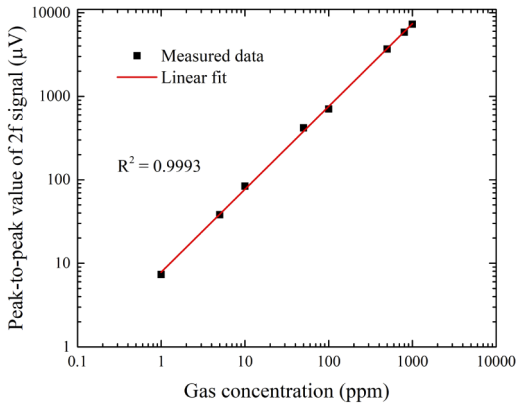

Fig. 8. The peak-to-peak value of the 2f signal as a function of ethane concentration.

The system stability was tested by repeatedly scanning the pump wavelength across the absorption line of ethane at 3348.15 nm and the results for 1000 ppm ethane balanced with nitrogen with a pump power of ~1.5 mW are shown in Fig. 9. During the stability experiment, the gas cell keeps being filled with ethane slowly (5 SCCM) to maintain constant gas concentration. The peak-to-peak value of the 2f signal varies ~ 2.2% over a period of 8 hours. This instability is believed to due mainly to pump power fluctuation in the HCF since the weak reflections of the pump at the HCF/SMF joints would interfere with the main pump beam and cause pump power fluctuation within the FPI cavity.

Table 1 summarizes the performance of MIR gas sensors with HCF gas cells. The NEA is given here for a fair comparison, which is independent of gas type and absorption strength. The last three rows are the results of this work for different integration time. The current work achieves the smallest NEA (for 410 s), which is about one order of magnitude better than the state-of-the-art MIR HCF gas sensors [26]. Our system is simple, compact and has good long-term stability, which is essential for practical applications.

Table 1. Performance of MIR HCF gas sensors[a]

Gas	Gas cell	Wavelength	Technique	Length	NEA	Integration time
N_2O [26]	HC-NCF	3.60 μm	DAS	120 cm	3.0×10^{-5}	40s
Methane [27]	Kagome HCF	3.33 μm	TDLAS	130 cm	4.6×10^{-4}	Not stated
Methane [28]	Kagome HCF	3.33 μm	CLaDS	130 cm	4.0×10^{-4}	1s
N_2O [29]	Revolver HCF	4.53 μm	TDLAS	320 cm	1.2×10^{-4}	1s
N_2O [18]	Capillary Fiber	4.46 μm	PTI-MZI	25.0 cm	5.1×10^{-4}	150s
Formaldehyde [19]	HC-NCF	3.60 μm	PTI-MZI	120 cm	9.2×10^{-5}	Not stated
Ethane (this work)	HC-NCF	3.34 μm	PTI-FPI	14.0 cm	1.0×10^{-5}	1s
					3.5×10^{-6}	100s
					2.0×10^{-6}	410s

[a]CLaDS: chirped laser dispersion spectroscopy

Optics EXPRESS

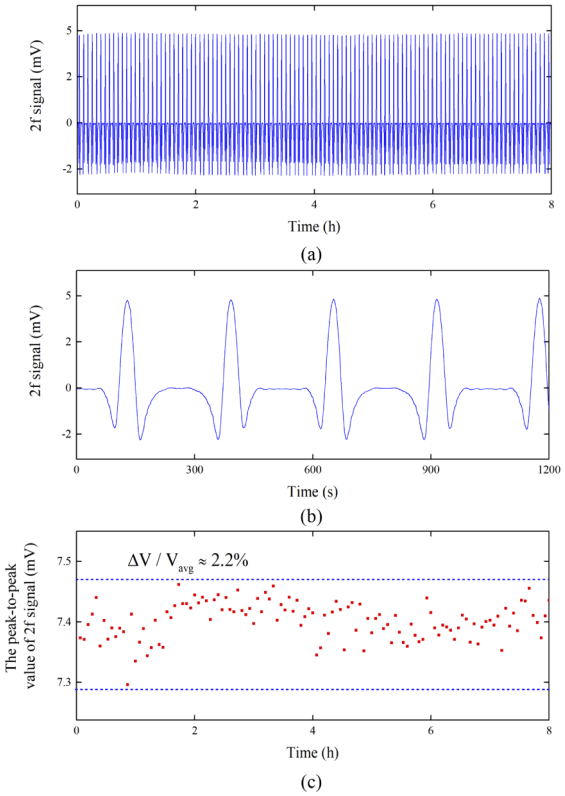

Fig. 9. Results of long-term stability test. (a) 2f lock-in output signal over a period of 8 hours. (b) 2f signal over a period of 1200 seconds. (c) The variation of the peak-to-peak value of the 2f signal over 8 hours.

5. Conclusion

In summary, we have reported a stable, compact, and highly sensitive ethane sensor with an HC-NCF gas cell that transmits both MIR and NIR signals with low loss. By launching the MIR pump and the NIR probe into the gas cell simultaneously from the opposite ends of the HCF, the separation of the MIR pump optics and the NIR probe circuit is achieved. Such a design of gas cell allows the use of a MIR pump to access the strongest absorption lines to generate larger PT phase modulation and a cost-effective NIR probe interferometer to detect the phase modulation with high sensitivity. With a 14-cm-long HC-NCF gas cell, a 3348.15 nm pump laser, and a 1550 nm probe FPI stabilized at quadrature, we demonstrated ethane detection with NEC of 13 ppb for 1 s lock-in time constant. The NEC goes down to 2.6 ppb for 410 s averaging time, corresponds to NEA of 2.0×10^{-6}, the smallest among all the MIR HCF gas sensors reported so far, to the best of our knowledge. The system instability is about 2.2% over a period of 8 hours. The high sensitivity, high stability, and simple structure of the detection system are promising for field applications. The sensitivity and stability could be further improved by optimizing the gas cell design to enhance the fringe contrast for probe FPI and to reduce the interference effect due to residual pump reflections. Similar sensing systems may be implemented for many other gases that have strong absorption in the MIR.

Funding

Hong Kong SAR government GRF grant (15220119); National Key Research and Development Program of China (2019YFB2203904); National Natural Science Foundation of China (61827820,

Optics EXPRESS

61535004, 62005233); China Postdoctoral Science Foundation (2019M663120); Hong Kong Polytechnic University (YW4C).

Disclosures

The authors declare no conflicts of interest.

References

1. Y. Xiao, J. A. Logan, D. J. Jacob, R. C. Hudman, R. Yantosca, and D. R. Blake, "Global budget of ethane and regional constraints on US sources," J. Geophys. Res. **113**(D21), D21306 (2008).
2. I. J. Simpson, F. S. Rowland, S. Meinardi, and D. R. Blake, "Influence of biomass burning during recent fluctuations in the slow growth of global tropospheric methane," Geophys. Res. Lett. **33**(22), L22808 (2006).
3. B. Hirst, G. Gibson, S. Gillespie, I. Archibald, O. Podlaha, K. D. Skeldon, J. Courtial, S. Monk, and M. Padgett, "Oil and gas prospecting by ultra-sensitive optical gas detection with inverse gas dispersion modeling," Geophys. Res. Lett. **31**, L12115 (2004).
4. P. Paredi, S. A. Kharitonov, and P. J. Barnes, "Elevation of exhaled ethane concentration in asthma," Am. J. Respir. Crit. Care Med. **162**(4), 1450–1454 (2000).
5. B. K. Puri, B. M. Ross, and I. H. Treasaden, "Increased levels of ethane, a non-invasive, quantitative, direct marker of n-3 lipid peroxidation, in the breath of patients with schizophrenia," Prog. Neuro-Psychopharmacol. Biol. Psychiatry **32**(3), 858–862 (2008).
6. K. Skeldon, L. McMillan, C. Wyse, S. Monk, G. Gibson, C. Patterson, T. France, C. Longbottom, and M. Padgett, "Application of laser spectroscopy for measurement of exhaled ethane in patients with lung cancer," Resp. Med. **100**(2), 300–306 (2006).
7. C. S. Patterson, L. C. McMillan, C. Longbottom, G. M. Gibson, M. J. Padgett, and K. D. Skeldon, "Portable optical spectroscopy for accurate analysis of ethane in exhaled breath," Meas. Sci. Technol. **18**(5), 1459–1464 (2007).
8. A. Sampaolo, S. Csutak, P. Patimisco, M. Giglio, G. Menduni, V. Passaro, F. K. Tittel, M. Deffenbaugh, and V. Spagnolo, "Methane, ethane and propane detection using a compact quartz enhanced photoacoustic sensor and a single interband cascade laser," Sens. Actuators, B **282**, 952–960 (2019).
9. P. Patimisco, G. Scamarcio, F. K. Tittel, and V. Spagnolo, "Quartz-enhanced photoacoustic spectroscopy: a review," Sensors **14**(4), 6165–6206 (2014).
10. C. C. Davis and S. J. Petuchowski, "Phase fluctuation optical heterodyne spectroscopy of gases," Appl. Opt. **20**(14), 2539–2554 (1981).
11. S. E. Bialkowski, *Photothermal Spectroscopy Methods for Chemical Analysis*, vol. 177. John Wiley & Sons, 1996.
12. P. Russell, "Photonic crystal fibers," Science **299**(5605), 358–362 (2003).
13. F. Yang, W. Jin, Y. Cao, H. L. Ho, and Y. Wang, "Towards high sensitivity gas detection with hollow-core photonic bandgap fibers," Opt. Express **22**(20), 24894–24907 (2014).
14. W. Jin, Y. C. Cao, F. Yang, and H. L. Ho, "Ultra-sensitive all-fibre photothermal spectroscopy with large dynamic range," Nat. Commun. **6**(1), 6767 (2015).
15. Y. Lin, W. Jin, F. Yang, Y. Tan, and H. L. Ho, "Performance optimization of hollow-core fiber photothermal gas sensors," Opt. Lett. **42**(22), 4712–4715 (2017).
16. F. Yang, Y. Tan, W. Jin, Y. Lin, Y. Qi, and H. L. Ho, "Hollow-core fiber Fabry–Perot photothermal gas sensor," Opt. Lett. **41**(13), 3025–3028 (2016).
17. P. Zhao, Y. Zhao, H. Bao, H. L. Ho, W. Jin, S. Fan, S. Gao, Y. Wang, and P. Wang, "Mode-phase-difference photothermal spectroscopy for gas detection with an anti-resonant hollow-core optical fiber," Nat. Commun. **11**(1), 1–8 (2020).
18. Z. Li, Z. Wang, F. Yang, W. Jin, and W. Ren, "Mid-infrared fiber-optic photothermal interferometry," Opt. Lett. **42**(18), 3718–3721 (2017).
19. C. Yao, S. Gao, Y. Wang, P. Wang, W. Jin, and W. Ren, "MIR-pump NIR-probe fiber-optic photothermal spectroscopy with background-free first harmonic detection," IEEE Sens. J. **20**(21), 12709–12715 (2020).
20. C. Yao, Q. Wang, Y. Lin, W. Jin, L. Xiao, S. Gao, Y. Wang, P. Wang, and W. Ren, "Photothermal CO detection in a hollow-core negative curvature fiber," Opt. Lett. **44**(16), 4048–4051 (2019).
21. S. Gao, Y. Wang, W. Ding, D. Jiang, S. Gu, X. Zhang, and P. Wang, "Hollow-core conjoined-tube negative-curvature fibre with ultralow loss," Nat. Commun. **9**(1), 2828 (2018).
22. S. Gao, Y. Wang, and P. Wang, "Silica-based modeless hollow-core fiber for broadband mid-IR guidance," in *2017 Conference on Lasers and Electro-Optics Pacific Rim (CLEO-PR)*, (IEEE, 2017), pp. 1–2.
23. H. Bao, Y. Hong, W. Jin, H. L. Ho, C. Wang, S. Gao, Y. Wang, and P. Wang, "Modeling and performance evaluation of in-line Fabry-Perot photothermal gas sensors with hollow-core optical fibers," Opt. Express **28**(4), 5423–5435 (2020).
24. R. Holmes, G. R. Jones, and N. Pusat, "Vibrational relaxation in propane, propylene, and ethane," J. Chem. Phys. **41**(8), 2512–2516 (1964).
25. Y. L. Hoo, S. J. Liu, H. L. Ho, and W. Jin, "Fast response microstructured optical fiber methane sensor with multiple side-openings," IEEE Photonics Technol. Lett. **22**(5), 296–298 (2010).

Optics EXPRESS

26. C. Yao, S. Gao, Y. Wang, P. Wang, W. Jin, and W. Ren, "Silica hollow-core negative curvature fibers enable ultrasensitive mid-infrared absorption spectroscopy," J. Lightwave Technol. **38**(7), 2067–2072 (2020).
27. M. Nikodem, K. Krzempek, G. Dudzik, and K. Abramski, "Hollow core fiber-assisted absorption spectroscopy of methane at 3.4 µm," Opt. Express **26**(17), 21843–21848 (2018).
28. K. Krzempek, K. Abramski, and M. Nikodem, "Kagome Hollow Core Fiber-Based Mid-Infrared Dispersion Spectroscopy of Methane at Sub-ppm Levels," Sensors **19**(15), 3352 (2019).
29. M. Nikodem, G. Gomolka, M. Klimczak, D. Pysz, and R. Buczynski, "Demonstration of mid-infrared gas sensing using an anti-resonant hollow core fiber and a quantum cascade laser," Opt. Express **27**(25), 36350–36357 (2019).